RSC Advances

PAPER

View Article Online
View Journal | View Issue

Cite this: *RSC Adv.*, 2022, **12**, 15470

Ion-imprinted guanidine-functionalized zeolite molecular sieves enhance the adsorption selectivity and antibacterial properties for uranium extraction†

Zhao Yi,[ab] Li Junwen,[a] Wu Sijin[a] and Cheng Haiming *[ab]

The important properties in the development of adsorbents for uranium extraction from seawater include specific selectivity to uranium ions and anti-biofouling ability in the ocean environment. In this paper, we report a novel strategy for efficient selective extraction of uranium from aqueous solutions and good anti-bacterial properties by surface ion-imprinted zeolite molecular sieves. Guanidine-modified zeolite molecular sieves 13X (ZMS-G) were synthesized and used as the support for the preparation of uranium(VI) ion-imprinted adsorbents (IIZMS-G) by ligands with phosphonic groups. The prepared IIZMS-G adsorbent was characterized *via* Fourier transform infrared spectroscopy (FT-IR), scanning electronic microscopy (SEM), X-ray diffraction (XRD), and energy dispersive spectroscopy (EDS). The results showed that guanidine groups have been successfully introduced onto the support while its morphology structure was maintained. The adsorption performance and selectivity to U(VI) ions, antibacterial property, and reusability of IIZMS-G were evaluated. The results showed that the maximum adsorption capacity reached 141.09 mg g^{-1} when the initial concentration of metal ions was 50 mg L^{-1} at pH 6 and 20 °C. The adsorption process followed the pseudo-second-order kinetic model and Langmuir adsorption isotherm model. The IIZMS-G exhibits an efficient selective adsorption of U(VI) ions from aqueous solutions with competing ions. In addition, the IIZMS-G exhibited excellent inhibitory effects on *Escherichia coli* and *Staphylococcus aureus*, and the inhibitory rate was 99.99% and 98.96% respectively. These results suggest that the prepared IIZMS-G adsorbent may promote the development strategy of novel high selectivity and antifouling adsorbents for uranium recovery from seawater.

Received 14th March 2022
Accepted 14th May 2022

DOI: 10.1039/d2ra01651f

rsc.li/rsc-advances

1. Introduction

Nuclear energy is reported as the best alternative cleaner energy to conventional fossil fuels.[1] Uranium is a wide nuclear resource for nuclear power generation.[2] However, uranium resource reserves on land are limited and a temporary supply can only be maintained for less than one century.[3] On the other hand, it has been reported that the total amount of uranium in seawater is nearly 4.5 billion tons, which is around 1000 times larger than the total uranium in land mines, even though seawater has a uranium concentration of only 3.3 ppb.[3] Therefore, many countries and scientists pay a lot attention to extracting uranium from seawater.[4–7] Nowadays extracting uranium from seawater by adsorption processes is considered as the most promising method due to its convenient operation, low cost, good reusability and wonderful extraction efficiency.[8,9] However, the efficient extraction of uranium from seawater is still a huge challenge due to the extremely low concentration of uranium (approximately 3.3 ppb),[10] many competitive ions in the oceans,[11] and the biofouling environment.[12]

In order to achieve the adsorbents with both high adsorption performance and good selectivity to uranium(VI) (U(VI)) ions, specific affinity ligands have been developed such as amidoxime,[13] oximes, amines/imines,[14] phosphoramides,[13] and phosphonates groups.[15,16] Yousef *et al.*[17] applied acid cured phosphate rock for uranium adsorption, the maximum adsorption capacity of uranium was up to 125 mg g^{-1}. An ordered mesoporous polymer–carbon composite containing phosphoric acid groups were prepared by Zhou *et al.*[18] showed the maximum adsorption capacity for uranium up to 274.15 mg g^{-1}. However, it is hard to obtain an efficient U(VI) selectivity by these ligands since there are several metal ions in the ocean environment will compete with the target uranium ions. In recent decades, surface ion-imprinted technology has been

[a]*The Key Laboratory of Leather Chemistry and Engineering of Ministry of Education, Sichuan University, Chengdu 610065, China*

[b]*National Engineering Laboratory for Clean Technology of Leather Manufacture, Sichuan University, Chengdu 610065, Sichuan, China. E-mail: chenghaiming@scu.edu.cn*

† Electronic supplementary information (ESI) available: Details of the adsorption isotherms, adsorption kinetics fitting data. See https://doi.org/10.1039/d2ra01651f

applied to enhance the selectivity to target metal ions in the field of wastewater treatment and uranium adsorption.[19] Ion-imprinted polymers (IIPs) are usually prepared by the copolymerization of a functional ligand and a cross-linker in the presence of template ions.[20] The IIPs can extract the target ions with good selectivity due to its memory effect on the template ions.[21,22] Mesoporous silica is a promising matrix owing to its high specific surface area, mechanical and thermal stability, chemical and irradiation durability, and easy organic modification.[22–24]

Moreover, the biofouling problems have been concerned for the development of uranium extraction adsorbents. Various ocean microorganisms will adhere to the surface of the adsorbent during several weeks immersed them in seawater, which will decrease the adsorption performance and the stability of adsorbent.[11] The development of good antimicrobial adsorbents should be a potential strategy to prevent the biofouling. Several antibacterial materials, including inorganic nanoparticles, small organic agents, and polymers, have been introduced onto the uranium extraction adsorbents.[12,25–28] In our previous work,[12,25] inorganic nanoparticles, TiO_2 and ZnO loaded amidoximated wool fibers showed good inhibition to the growth of aerobic bacteria, anaerobic bacteria, fungus, and mildew with good uranium adsorption capacity. Moreover, organic groups such as quaternary ammonium derivatives and guanidine derivatives have been employed onto the adsorbents.[27,28] Guanidine derivatives are a potential candidate for preparing antibacterial adsorbents because it can maintain protonation in a wide range of pH in polar solvents and destroy the normal metabolism of organisms.[29,30]

In this report, zeolite molecular sieves (ZMS-13X) were modified with (3-aminopropyl)triethoxysilane (APTES), and then reacted with cyanamide to obtain guanidine-modified zeolite molecular sieve (ZMS-G). ZMS-G was further applied as the support for preparing ion imprinted material (IIZMS-G) using uranium as the template ion and vinyl phosphoric acid (VPA) as the functional ligand. The prepared IIZMS was applied for U(VI) adsorption in batch experiments; in which adsorption parameters, adsorption kinetics, and adsorption equilibrium were evaluated. Moreover, the competing adsorption of the adsorbent towards U(VI), Ca(II), Mg(II), Zn(II), and Cu(II) were investigated. The antibacterial properties of IIZMS-G have been investigated *via* cultured with *S. aureus* and *E. coli*. In simulated seawater, the adsorption capacity of adsorbent materials for uranium ions was explored.

2. Experimental

2.1. Reagents and materials

Zeolite molecular sieves 13X (ZMS-13X), cyanamide (NH_2–C≡N), vinyl phosphonic acid (VPA), (3-aminopropyl)triethoxysilane (APTES), ethylene glycol dimethacrylate (EGDMA), and 2,2′-azobisisobutyronitrile (AIBN) were purchased from Aladdin (Shanghai, China). All other reagents were analytic grade and used as received without further purification. The stock solution of U(VI) (1000 mg L^{-1}) was prepared by dissolving appropriate amount of $UO_2(NO_3)_2 \cdot 6H_2O$ in deionized water (18.2 MΩ).

2.2. Modification of ZMS with guanidine groups

The guanidine functionalized ZMS-13 (ZMS-G) were synthesized by coupling with (3-aminopropyl)triethoxysilane (APTES) and then reacted with cyanamide (NH_2–C≡N) (Scheme 1). The APTES modified ZMS-13X was prepared according to the reported with some modifications.[31] Briefly, 2.0 g of ZMS-13X (particle size 0.5–1.5 μm) was suspended in 50 mL of methylbenzene, and then 8.0 mL of APTES was added. The mixture was refluxed under magnetic stirring at 110 °C for 24 h in N_2 atmosphere. After that, the suspended solids were filtered out and thoroughly washed with ethanol. The obtained product was assigned as ZMS-APTES. Then, to introduce guanidine groups,

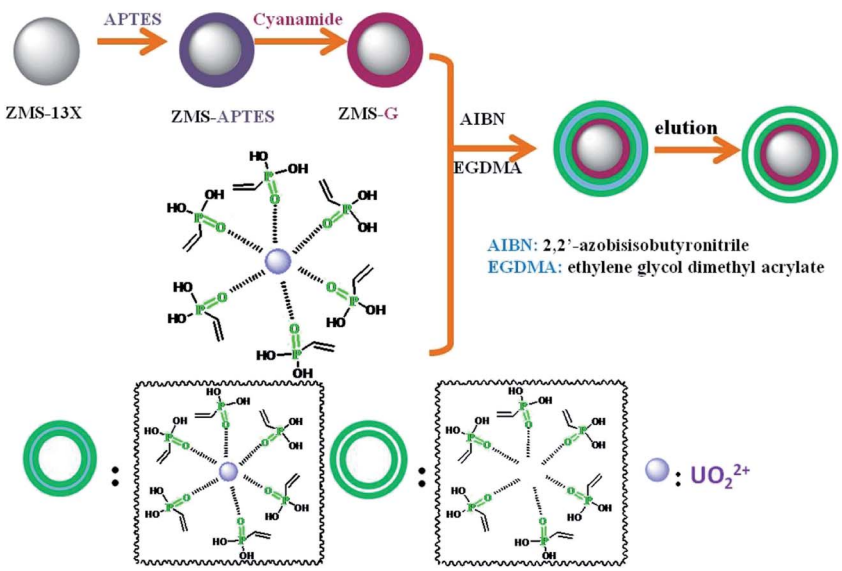

Scheme 1 The schematic diagram of preparation process of IIZMS-G.

the prepared ZMS-APTES was dispersed with 50 mL of 95% ethanol, 3.5 mL of NH_2–C≡N, and 3.0 mL of HCl (12 mol L^{-1}). The mixture was refluxed under magnetic stirring at 120 °C for 20 min, and then 0.6 mL of HCl (12 mol L^{-1}) was slowly added to the mixture and keeps reacting for another 10 min. After that, the solids were filtered out and thoroughly washed with 95% ethanol. The obtained product was assigned as ZMS-G.

2.3. Preparation of surface ion-imprinted ZMS-G

The surface ion imprinting on ZMS-G was synthesized through a free radical co-precipitation polymerization method. A typical preparation procedure of IIZMS-G is described as follows: 0.1 mmol of $UO_2(NO_3)_2 \cdot 6H_2O$ and 8 mmol of vinyl phosphonic acid (VPA) were dissolved in 45 mL of ethanol/acetone (2 : 1, v/v) by stirring at room temperature for 30 min to form the U(VI) and VPA complex. Then, 1.0 g of ZMS-G, 2.0 mL of ethylene glycol dimethacrylate (EGDMA), and 0.1 g of AIBN were added to co-precipitation polymerization of U(VI) ion imprinted polymers onto the ZMS-G. The mixture was stirred at 70 °C for 24 h in N_2 atmosphere. After that, the suspended solids were filtered out and thoroughly washed with ethanol. 0.1 mol L^{-1} of H_2SO_4 was used for eluting the imprinted U(VI) ions. The prepared solids were desiccated at 65 °C and designed as IIZMS-G. For comparison, a non-imprinted adsorbent was prepared as the above mentioned steps in the absence of $UO_2(NO_3)_2 \cdot 6H_2O$ and the elution step, which was designed as NIZMS-G.

2.4. Characterization

FT-IR spectra were recorded in the range of 4000–400 cm^{-1} with a resolution of 2 cm^{-1} by a Nicolet Is10 Fourier transform infrared spectrometer (FT-IR) (Thermo Fisher Scientific, USA) using the potassium bromide particle method. The samples were analyzed in the range of 5° to 90° using an X-ray diffraction analyzer of the EMPYREAN model (PANalytical B.V., Netherland). Surface morphology of the samples was observed using a JSM7500F scanning electron microscope (SEM) (JEOL, Japan). The elemental composition of the samples was measured by 51-XMX0019X-Max energy-dispersive X-ray spectroscopy (EDXS) (Oxford Instruments, UK). The zeta potential of the sample was detected with a Zetasizer Nano ZSP (Malvern, UK), the concentration of the prepared suspension is 0.5 mg mL^{-1}, and the pH of the suspension was adjusted with 0.01 M sodium hydroxide or hydrochloric acid solution.

2.5. Batch adsorption experiments

The batch experiments of IIZMS-G adsorption of U(VI) ions were investigated in a serious of 50 mL polyethylene tubes. A typical adsorption process was described as follows: 10 mg of the adsorbent and 30 mL of U(VI) ion solution (50 mg L^{-1}) were added in the tube and incubated at 20 °C by shaking for 300 min until the achievement of equilibrium. The pH of the solution was adjusted to a desired value by solutions of HCl (0.1 mol L^{-1}) or NaOH (0.1 mol L^{-1}). After adsorption, the adsorbents were spin down, and the concentration of U(VI) ion in the supernatant was determined by a 5100 inductively coupled plasma-optical emission spectrometry (ICP-OES, Agilent, USA). The adsorption capacity q_e (mg g^{-1}) was calculated by eqn (1):

$$q_e = \frac{(C_0 - C_e) \times V}{m} \quad (1)$$

where C_0 (mg L^{-1}) and C_e (mg L^{-1}) are the initial and equilibrium concentrations of the metal ions, respectively; V (L) is the volume of the testing solution and m (g) is the weight of adsorbent. All the adsorption experiments were repeated three times.

To evaluate the selectivity of IIZMS-G, 10 mg of the adsorbent was stirred at 20 °C with 30 mL of the solution containing both U(VI) ion and Zn(II), Cu(II), Mg(II), Ca(II) ions at pH 4.3, where the concentration of each metal ion was 50 mg L^{-1}. After adsorption, the concentration of metal ions in the supernatant was determined by ICP-OES. The distribution ratio (K_d, L g^{-1}), selectivity coefficient K and the relative selectivity coefficient K' were calculated by eqn (2)–(4):

$$K_d = \frac{(C_0 - C_e)}{C_e} \times \frac{V}{m} \quad (2)$$

$$K_{U(VI)/M} = \frac{K_{d(U(VI))}}{K_{d(M)}} \quad (3)$$

$$K' = \frac{K_{IIZMS\text{-}G}}{K_{NIZMS\text{-}G}} \quad (4)$$

2.6. Antibacterial evaluation

In this study, *E. coli* and *S. aureus* were selected to evaluate the antimicrobial properties of NIZMS-G and IIZMS-G. Briefly, bacteria were cultivated in their liquid lysogeny broth (LB) medium at 37 °C for 18 h then the cell suspensions were diluted with PBS (0.03 mol L^{-1}, pH 7.2–7.4) to cell density (counted in colony-forming units (CFU)) of 4×10^4 CFU mL^{-1}. 50 mg of IIZMS-G, 49 mL of PBS, and 1 mL of cell suspensions was put into a 150 mL flask, keeping cell concentration at 4×10^4 CFU mL^{-1}. Then the flask was shaken on a thermostat shaker at 37 °C for 3 h exposed under visible light. Subsequently, 1.0 mL of cell suspensions was taken out for preparing a series of tenfold dilution with PBS, plated out in LB agar. The plates were incubated at 37 °C for 18 h and then counted their colony-forming units. As the control, only bacterial suspension was added during the test. The reduction of CFU (X) was calculated by eqn (5):

$$X(\%) = \frac{(A - B)}{A} \times 100\% \quad (5)$$

where A is average number of bacterial colonies in the control, and B is average number of bacterial colonies on samples.

2.7. Desorption and regeneration study

The IIZMS-G after adsorption of U(VI) ions was weighed into a 50 mL beaker, and 0.1 mol L^{-1} H_2SO_4 was added for elution until U(VI) ions could not be detected in the solution. The desorbed IIZMS-G was obtained by centrifugation, washed with ultrapure water until neutral, and dried at 65 °C. Add 10.0 mg of

the above IIZMS-G to 30.0 mL of pH 5.5, 50 mg L^{-1} U(VI) ion solution, and place it at 20 °C under magnetic stirring for 150 min. After reaching the adsorption equilibrium, the concentration of U(VI) ions in the solution was measured and the adsorption capacity was calculated. After five cycles, the regeneration performance of IIZMS-G was investigated.

3. Results and discussion

3.1. Characterization

FT-IR spectra were recorded by a Nicolet Is10 Fourier transform infrared spectrometer (Thermo Fisher Scientific, USA) (Fig. 1). The FT-IR spectrum of ZMS-13X showed peaks at 3486 cm^{-1}, and 1639 cm^{-1} belong to the stretching vibration and the bending vibration of hydroxyl group. The peak at 1446 cm^{-1} belongs to carbonate,[32] the peaks at 750 cm^{-1} and 977 cm^{-1} ascribe to the stretching vibration of Si–O–Si, while peak at 563 cm^{-1} belongs to the stretching vibration of Si–O[33] (Fig. 1a). In comparison with the ZMS-13X, the broadening of the peak at 3486 cm^{-1} is ascribed to the stretching vibration of N–H, and a new peak appeared at 2927 cm^{-1} is ascribed to the stretching vibration of C–H, indicated the successful graft of APTES onto ZMS-13X (Fig. 1b). Fig. 1c showed a broadening peak at 1639 cm^{-1} (the stretching vibration of C=N) and the broadening peak at 977 cm^{-1} to 1022 cm^{-1} (stretching vibration of C–N),[27] suggesting that guanidine groups has been successfully introduced onto the ZMS-13X. The peak at 1729 cm^{-1} belongs to stretching vibration of C=O,[34] 1461 cm^{-1} and 1386 cm^{-1} are C–H bending vibration peaks, which belongs to the cross-linking agent EGDMA. The peak at 1045 cm^{-1}, 1147 cm^{-1} and 1249 cm^{-1} are P–O and P=O stretching vibration peaks in phosphonic acid group.[35,36] In summary, the IIZMS-G adsorbent had been successfully prepared.

The XRD patterns of ZMS-13X and IIZMS-G samples are shown in Fig. 2. The 2θ peaks in the region of 10 to 30.9° are typical faujasite structures, which corresponding to the pore structure of ZMS-13X (Fig. 2a).[37] After grafting with APTES and guanidine groups, the pore structure of ZMS-13X was unchanged, merely the intensity of diffraction peaks decrease slightly (Fig. 2b and c), which may be caused by the surface of the lattice structure covered with amorphous organic matter.[38] After the surface was ion imprinted, most of the diffraction peaks disappeared and an amorphous broad peak occur, which

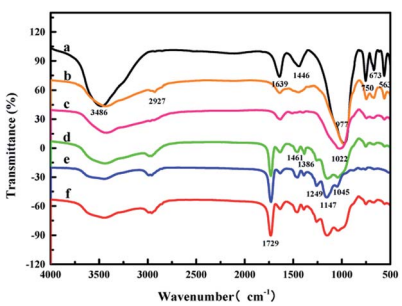

Fig. 1 FT-IR spectra of (a) ZMS-13X, (b) ZMS-APTES, (c) ZMS-G, (d) U(VI)-IIZMS-G, (e) IIZMS-G, and (f) NIZMS-G.

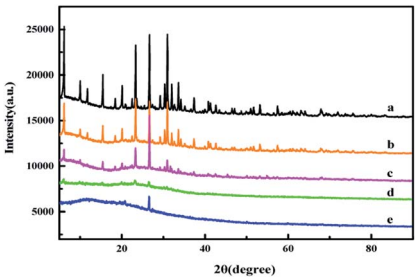

Fig. 2 The XRD spectra of (a) ZMS-13X, (b) ZMS-APTES, (c) ZMS-G, (d) U(VI)-IIZMS-G, and (e) IIZMS-G.

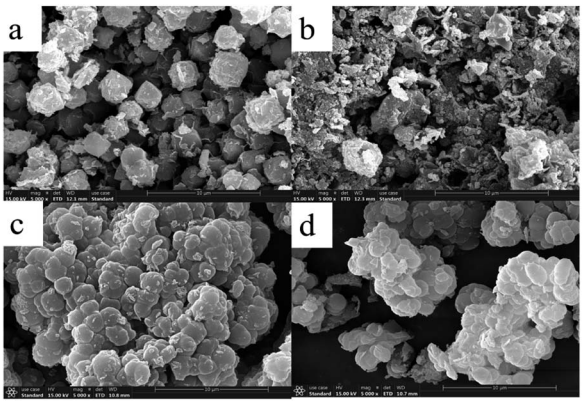

Fig. 3 The SEM images of (a) ZMS-13X, (b) ZMS-G, (c) IIZMS-G, and (d) NIZMS-G.

may be due to the covering of the imprinted polymer onto the surface (Fig. 2d and e).

The morphological images of ZMS-13X, ZMS-G, IIZMS-G and NIZMS-G were observed by a JSM 7500F scanning electron microscopy (SEM) (JEOL, Japan) and show in Fig. 3. Octahedral structure was observed clearly for ZMS-13X (Fig. 3a), which is consistent with the previous reports.[39] However, after functionalized with guanidine groups, tremendous of polymer accumulations can be observed on the surface of ZMS-G (Fig. 3b), indicating a successfully graft of guanidine groups onto ZMS-13X. After imprinting polymerization on the surface of ZMS-G, a large number of spherical agglomerates appeared on the surfaces of IIZMS-G and NIZMS-G (Fig. 3c and d). However the morphology of IIZMS-G was rougher and looser than that of NIZMS-G, which may be due to the removal of template ions. The elemental compositions of the samples were measured *via* 51-XMX0019 X-Max energy dispersive spectrometer (EDS) (Oxford Instruments, UK) (Fig. 4). It can be seen that the main elements of U(VI)-IIZMS-G were C, O, Na, Al, Si, P, Cl and U (2.77% wt) (Fig. 4a). After elution, the characteristic peak of U element on the energy spectrum disappeared. The results illustrate that the template U(VI) ions could be eluted thoroughly by 0.1 mol L^{-1} of H_2SO_4.

3.2. U(VI) adsorption performance

3.2.1. Effect of pH. The effects of pH on adsorption of IIZMS-G for U(IV) ions was performed in 50 mL polyethylene

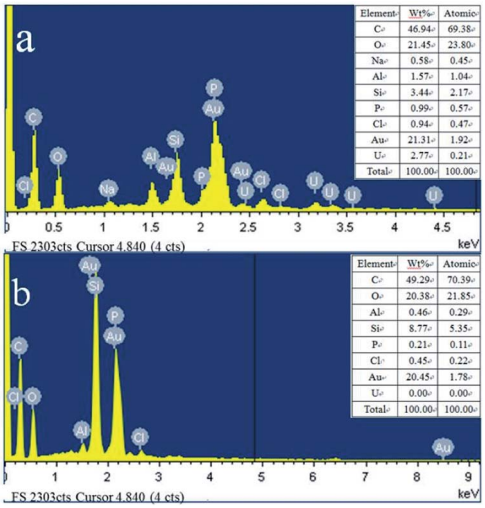

Fig. 4 The EDS images of (a) U(VI)-IIZMS-G, (b) IIZMS-G.

tubes containing with 10 mg of adsorbent at 20 °C for 300 min by varying the initial pH of the solution from 3.0 to 9.0 (Fig. 5a). It can be observed that the uptake of U(VI) by NIZMS-G was much lower than by IIZMS-G under the same pH value. The uptake of U(IV) by IIZMS-G increased from 17.32 mg g^{-1} to 163.71 mg g^{-1} with the increase in pH from 3.0 to 6.0; after that the uptake of U(IV) ions decreased with the initial pH increasing to 9.0. The initial pH of the solution plays roles in both the surface charge of the adsorbent and the ionic species of U(IV) in the solution as well. The isoelectric point of IIZMS-G is at 5.4 (Fig. S1†). There are two reasons may cause the adsorption process depending on the pH of the solution. One reason may be owing to that, while the pH is lower than 3.0, the phosphonic groups on IIZMS-G surface were protonated and U(VI) cationic species had to compete with the protons, which might hinder the complexation between U(IV) ions and the functional groups,[40] while with the pH increased, phosphonic groups would be gradually deprotonated and the surface of the IIZMS-G becomes more negatively charged, which would increase its binding ability to positively charged U(VI) ions. The other reason is that U(VI) exists in different species dependent on pH of the solution. Uranyl ions (UO_2^{2+}) were the dominant species when the pH was lower than 3.0, while the pH of the solution increased from 4.0 to 6.0, the phosphate group gradually deprotonated, and UO_2^{2+} was gradually hydrolyzed into the main $UO_2(OH)^+$, $(UO_2)_2(OH)_2^{2+}$, $(UO_2)_3(OH)_4^{2+}$, $(UO_2)_3(OH)^{5+}$ and $(UO_2)_4(OH)^{7+}$ ions,[40] all of which are positively charged ionic forms that are easy to coordinate with phosphate groups, making IIZMS-G adsorption capacity increased. As the pH of the solution increased from 6.0 to 9.0, UO_2^{2+} was further hydrolyzed to $UO_2(OH)_2$ precipitation and negatively charged ionic forms, including the main $UO_2(OH)_3^-$, $UO_2(OH)_4^{2-}$, $(UO_2)_3(OH)_7^-$, $(UO_2)_3(OH)_8^{2-}$, $(UO_2)_3(OH)_8^{2-}$ and $(UO_2)_3(OH)_{10}^{4-}$ ions,[40] with phosphoric acid on the surface of IIZMS-G the electrostatic repulsion of the groups leads to a decrease in the adsorption capacity.

3.2.2. Adsorption kinetics. The effect of contact time on the adsorption of IIZMS-G for U(IV) ions was studied in 50 mL PE tubes containing 30 mL of 50 mg L^{-1} uranium(VI) solution with 10 mg of adsorbent at 20 °C and pH 5.5. The relationship between adsorption amount (q_t) and contact time (t) is shown in Fig. 5b. It could be observed that the rate of adsorption U(VI) ions onto both IIZMS-G and NIZMS-G was rapid during the first 100 min, and then gradually reaches equilibrium at around 150 min. The adsorption capacity at equilibrium is 141.09 mg g^{-1} (IIZMS-G) and 40.45 mg g^{-1} (NIZMS-G), respectively. It is

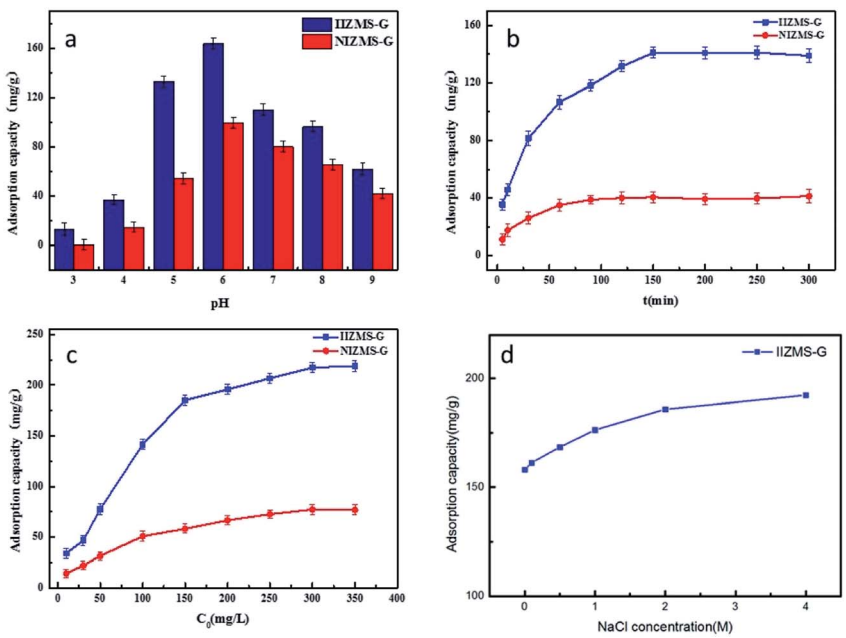

Fig. 5 U(VI) adsorption by IIZMS-G. (a) Initial pH, (b) contact time, (c) initial concentration of U(VI), (d) NaCl concentration.

Table 1 Kinetic parameters for U(VI) adsorption by IIZMS-G and NIZMS-G

	Pseudo-first-order			Pseudo-second-order		
Sample	q_e (mg g^{-1})	k_1 (min^{-1})	R^2	q_e (mg g^{-1})	k_2 (mg g^{-1} min^{-1})	R^2
IIZMS-G	115.65	2.00×10^{-2}	0.9867	151.29	2.98×10^{-4}	0.9906
NIZMS-G	37.37	3.50×10^{-2}	0.9910	45.87	1.21×10^{-3}	0.9956

clearly shown that the adsorption amount of U(VI) ions onto IIZMS-G is always higher than that onto NIZMS-G, indicating that IIZMS-G has stronger affinity for U(VI) ions than NIZMS-G. To ensure the adsorption process reaches equilibrium, the subsequent experiments were performed with 300 min.

The FT-IR spectrum of IIZMS-G after adsorption showed a shift in the P–O peak from 1053 cm^{-1} to 1148 cm^{-1} and O–P–O peak from 561 cm^{-1} to 553 cm^{-1}, while a new peak appeared at 881 cm^{-1} is ascribed to $[O{=}U{=}O]^{2+}$ vibration (Fig. S2†).[41] Additionally, the emergence of a peak at 3.19 keV to uranium was observed in the EDS spectrum (Fig. S3†). These results illustrate that IIZMS-G successfully adsorbed uranium.

To further investigate the adsorption kinetics, the experimental data were fitted to two common kinetic models, the pseudo-first order and the pseudo-second order kinetic models. The fitting profiles are shown in Fig. S4† and the kinetic parameters are summarized in Table 1. The experimental data of adsorption U(VI) onto IIZMS-G fitted well with the pseudo-second-order model, with the correlation coefficient (R^2) value at 0.9906. The results reveals that the adsorption of U(VI) ions onto IIZMS-G is predominantly a chemical adsorption process.[42]

3.2.3. Adsorption isotherms. The effect of the initial concentration of U(VI) ions on the adsorption was investigated by varying the concentration from 10 to 350 mg L^{-1}. The experiments were carried out at 20 °C with 30 mL of U(VI) solution and pH 5.5 with 10 mg of adsorbent for 300 min. The results showed that the adsorption capacity increases with increasing the initial concentration of U(VI) (Fig. 5c). The adsorption amount of NIZMS-G is less than that of IIZMS-G while at the same adsorption conditions, suggesting that IIZMS-G has more effective adsorption sites than NIZMS-G. In order to elucidate the nature of the adsorption process and adsorption mechanism, the experimental data were evaluated with adsorption isotherm models, Langmuir model and Freundlich model.[43,44] The fitting results are shown in Fig. S5† and Table 2. It shows that the experimental data are fitted well with the Langmuir isotherm model, with the correlation coefficient (R^2) at 0.9969 (IIZMS-G) and 0.9918 (NIZMS-G), respectively, indicating a monolayer uniform adsorption mode for IIZMS-G adsorbing U(VI). The maximum U(VI) adsorption capacity (q_m) calculated by the Langmuir isotherm function was 234.74 mg g^{-1} (IIZMS-G) and 91.41 mg g^{-1} (NIZMS-G), respectively. The results further illustrate that the ion imprinting process can significantly increase the adsorption capacity of U(VI) ions onto IIZMS-G. Compared with literature, the adsorption capacity of this work is good and with good antibacterial properties, therefore, it is a promising adsorbent for uranium extraction from seawater (Table 3).

3.2.4. Effect of ionic strength. The effect of ionic strength on the adsorption of U(VI) on IIZMS-G was investigated (Fig. 5d). The results show that the high concentration of NaCl favors the adsorption of IIZMS-G on U(VI), which may be due to the fact that the cations adsorbed on the surface of the adsorbent will

Table 2 Parameters of Langmuir and Freundlich models for U(VI) adsorption by IIZMS-G and NIZMS-G

	Langmuir			Freundlich		
Sample	q_m (mg g^{-1})	K_L (L mg^{-1})	R^2	K_F (mg g^{-1})	$1/n$	R^2
IIZMS-G	218.90	5.29×10^{-2}	0.9969	28.82	0.40	0.9299
NIZMS-G	76.93	1.78×10^{-2}	0.9918	6.11	0.46	0.9860

Table 3 The adsorption capacity of IIZMS-G and the values of other literature comparison

Adsorbents	Experimental conditions	Q_m (mg g^{-1})	Antibacterial property	References
Aluminum oxide nanopowder	$T = 301$ K, pH = 5.0	13	Not shown	45
Chitosan modified phosphate rock	$T = 298$ K, pH = 2.5	8.06	Not shown	46
Phosphate rock	$T = 298.15$ K, pH = 5	125	Not shown	17
Mesoporous polymer–carbon composites	$T = 298$ K, pH = 4, 0.01 M $NaNO_3$	274.15	Not shown	18
p-PVB-PAA	pH 5, 293 K	207.02	Not shown	47
IIZMS-G	$T = 298$ K, pH = 6	218.90	Yes	This work

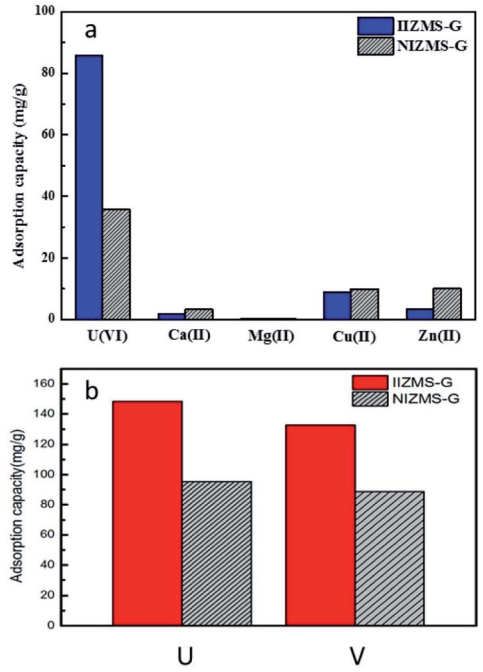

Fig. 6 (a) Adsorption capacity of IIZMS-G and NIZMS-G for U(VI) and Ca(II), Mg(II), Cu(II) and Zn(II) ions from mixed solution. (Adsorbent dosage: 10 mg, each metal ion concentration 50 mg L^{-1}, solution: 30 mL, *T*: 20 °C, pH: 4.3, *t*: 300 min). (b) Adsorption capacity of IIZMS-G and NIZMS-G for U(VI) and V(V). (Adsorbent dosage: 10 mg, metal ion concentration 50 mg L^{-1}, solution: 30 mL, *T*: 20 °C, pH: 6.0, *t*: 300 min).

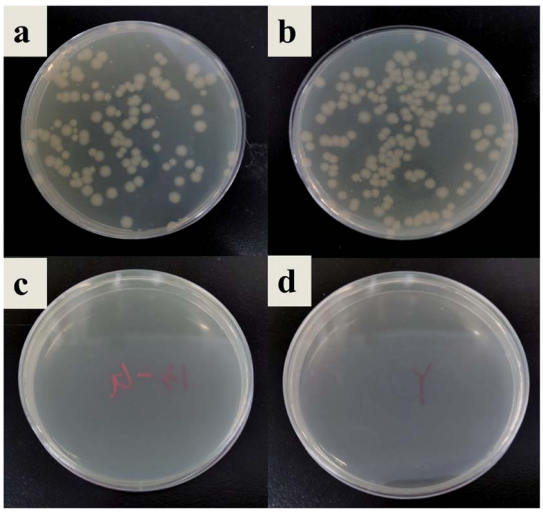

Fig. 7 Antibacterial test to *E. coli*. (a) Control, (b) ZMS-13X, (c) ZMS-13X-G, and (d) IIZMS-G.

generate a positively charged ion layer around the adsorben. The negatively charged layer forms an electrostatically diffused double layer. The increase in ionic strength leads to the compression of the diffusion bilayer on the surface of the adsorbent, which promotes electrostatic attraction and facilitates U(VI) adsorption.[48]

3.3. Effect of competing ions on uranium(VI) adsorption

Ion imprinting technique enhances the adsorbents with high selectivity to the target ions. The adsorption selectivity of IIZMS-G towards U(VI) ions were investigated by using 10 mg of the adsorbent with 30 mL of the solution containing 50 mg L^{-1} of U(VI) and coexisting ions at pH 4.3 and 20 °C for 300 min. In this study, U(VI), Zn(II), Cu(II), Mg(II) and Ca(II) were chosen as competitive metal ions because they are common ions in seawater. The adsorption capacity is shown in Fig. 6a and the data for the relative selectivity coefficient K' was summarized in Table 4. The value of K' beyond 3.0 demonstrates significance adsorption selectivity.[49] The results showed that the adsorption capacity of U(VI) on IIZMS-G was higher than the other competing metal ions (Cu(II), Zn(II), Ca(II), and Mg(II)). It implies that the specific imprinted cavities on IIZMS-G particle play an important role in the adsorption of U(VI) when competing with other ions. Furthermore, the values of K' are 6.94 (Ca(II)), 8.40 (Mg(II)), 3.97 (Cu(II)), and 11.23 (Zn(II)), respectively, suggesting that IIZMS-G exhibits excellent adsorption selectivity towards U(VI) ions.

Furthermore, vanadate ions (V(V)) will be competing with U(VI) ions in seawater. The competing adsorption of IIZMS-G towards U(VI) and V(V) ions were investigated at pH 6.0 and 20 °C for 300 min (Fig. 6b). The results showed that The results showed that the adsorption capacity of U(VI) (148.37 mg g^{-1}) on IIZMS-G was higher than that of V(V) (132.76 mg g^{-1}). Moreover, the ion-imprinted adsorbent showed higher adsorption amount on both ions, implying that ion-imprinting strategy should be an efficient technique for preparing uranium adsorbents.

3.4. Antibacterial evaluation

In this study, the antibacterial properties of IIZMS-G were investigated by exposuring them to 4×10^4 CFU mL^{-1} of *E. coli*

Table 4 K_d, K, K' parameters for IIZMS-G for competing adsorption

	IIZMS-G			NIZMS-G			
Metal ions	q_e (mg g^{-1})	K_d (L g^{-1})	K	q_e (mg g^{-1})	K_d (L g^{-1})	K	K'
U(VI)	85.82	1.64		35.87	0.46		
Ca(II)	1.69	1.88×10^{-2}	87.35	3.29	3.68×10^{-2}	12.59	6.94
Mg(II)	0.16	1.61×10^{-3}	1017.44	0.38	3.83×10^{-3}	121.10	8.40
Cu(II)	8.91	9.39×10^{-2}	17.46	9.96	0.11	4.40	3.97
Zn(II)	3.30	3.60×10^{-2}	45.51	10.10	0.11	4.05	11.23

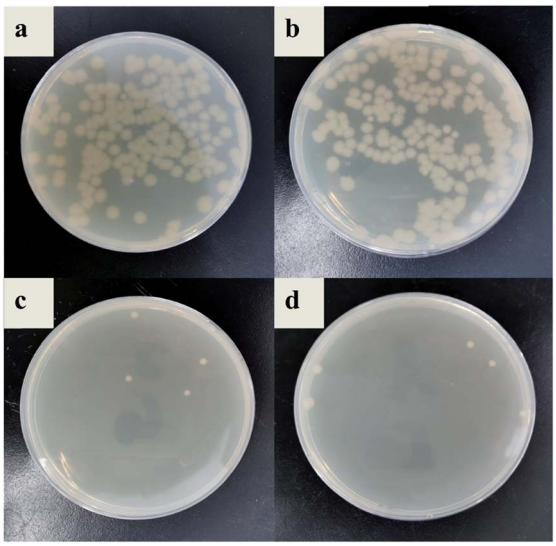

Fig. 8 Antibacterial test to *S. aureus*. (a) Control, (b) ZMS-13X, (c) ZMS-13X-G, and (d) IIZMS-G.

solution and *S. aureus* solution, respectively (Fig. 7 and 8). The results showed that the colony growth for control (Fig. 7a and 8a) and ZSM-13X (Fig. 7b and 8b) were very similar, illustrating that ZSM-13X had no antibacterial effect. After grafting guanidine on the surface of ZSM-13X, no colony could be observed (Fig. 7c and d). The results indicate that IIZMS-G was possessed of excellent antibacterial effect to *E. coli*, with the antibacterial rate to 99.99%; while to *S. aureus*, the antibacterial rate reached 98.96%.

3.5. Desorption and reusability study

To develop a batch treatment process, it is essential to describe regeneration aspects of the process in order to improve its cost effectiveness by recycling the adsorbent for reuse in multiple cycles (Fig. 9). H_2SO_4 solution (0.1 mol L^{-1}) was used as the elution agent. The adsorption–desorption cycles were conducted five times by using the same adsorbents. After 5 cycles, the adsorption capacity of the IIZMS-G decreased from 138.54 mg g^{-1} to 110.84 mg g^{-1} while the removal efficiency was still maintained above 80%. Furthermore, after 5 cycles, the antibacterial test showed that its antibacterial rate to *E. coli* and *S. aureus* still maintained at 90.23% and 95.18%, respectively. These results indicated IIZMS-G has a promising reusability for long-term uranium adsorption.

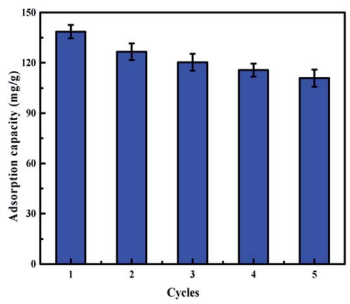

Fig. 9 Adsorption capacity of IIZMS-G after 5 cycles of adsorption and desorption process. (Adsorbent dosage: 10 mg, U(VI) ion concentration 50 mg L^{-1}, solution: 30 mL, *T*: 20 °C, pH: 5.5, *t*: 300 min).

4. Conclusion

In summary, guanidine-functionalized zeolite molecular sieve was synthesized and applied as the matrix for preparing surface ion-imprinted adsorbents IIZMS-G for U(VI) adsorption by radical-induced polymerization and the *in situ* co-precipitation method, where phosphonic acid groups were introduced as the binding groups for U(VI) ions. The prepared IIZMS-G was used to adsorption U(VI) ions from aqueous solution. The adsorption processes data followed the pseudo-second-order kinetic model and the Langmuir isotherm model. The maximum uranium adsorption capacity of IIZMS-APTES could be reached at 234.74 mg g^{-1} from the Langmuir isotherm model. In particular, IIZMS-G exhibited excellent antimicrobial properties to *E. coli* and *S. aureus*. Moreover, IIZMS-G illustrated efficient adsorption selectivity for U(VI) ions over coexisting metal ions. Therefore, this study provides an insight for constructing novel adsorbents to extracting uranium(VI) ions from seawater with good selectivity and antimicrobial properties.

Conflicts of interest

There are no conflicts to declare.

Acknowledgements

The authors are grateful for the financial support of the Natural Science Foundation of China (22178231).

References

1 IAEA, *OECD Uranium 2014: Resources, Production and Demand*, OECD/NEA Publishing, Paris, France, 2014.
2 A. Bleise, P. R. Danesi and W. Burkart, *J. Environ. Radioact.*, 2003, **64**, 93–112.
3 S. Brown, S. Chatterjee, M. J. Li, Y. F. Yue, C. Tsouris, C. J. Janke, T. Saito and S. Dai, *Ind. Eng. Chem. Res.*, 2016, **55**, 4130–4138.
4 R. V. Davies, J. Kennedy, R. W. McIlroy, R. Spence and K. M. Hill, *Nature*, 1964, **203**, 1110–1115.
5 A. D. Kelmers, *Sep. Sci. Technol.*, 1981, **16**, 1019–1035.
6 M. Tamada, *J. Jpn. Inst. Energy*, 2009, **88**, 249–253.
7 J. Kim, C. Tsouris, Y. Oyola, C. J. Janke, R. T. Mayes, S. Dai, G. Gill, L. J. Kuo, J. Wood, K. Y. Choe, E. Schneider and H. Lindner, *Ind. Eng. Chem. Res.*, 2014, **53**, 6076–6083.
8 H. Lindner and E. Schneider, *Energy Econ.*, 2015, **49**, 9–22.
9 J. Kim, C. Tsouris, R. T. Mayes, Y. Oyola, T. Saito, C. J. Janke, S. Dai, E. Schneider and D. Sachde, *Sep. Sci. Technol.*, 2013, **48**, 367–387.
10 C. W. Abney, R. T. Mayes, T. Saito and S. Dai, *Chem. Rev.*, 2017, **117**, 13935–14013.

11 J. Park, G. A. Gill, J. E. Strivens, L. J. Kuo, R. T. Jeters, A. Avila, J. R. Wood, N. J. Schlafer, C. J. Janke, E. A. Miler, M. Thomas, R. S. Addleman and G. T. Bonheyo, *Ind. Eng. Chem. Res.*, 2016, **55**, 4328–4338.
12 J. Wen, Q. Li, H. Li, M. Chen, S. Hu and H. Cheng, *Ind. Eng. Chem. Res.*, 2018, **57**, 1826–1833.
13 N. Tang, J. Liang, C. Niu, H. Wang, Y. Luo, W. Xing, S. Ye, C. Liang, H. Guo, J. Guo, Y. Zhang and G. Zeng, *J. Mater. Chem. A*, 2020, **8**, 7588–7625.
14 P. Yang, Q. Liu, J. Liu, R. Chen, R. Li, X. Bai and J. Wang, *J. Hazard. Mater.*, 2018, **363**, 248–257.
15 Z. Yin, J. Xiong, M. Chen, S. Hu and H. Cheng, *J. Radioanal. Nucl. Chem.*, 2016, **307**, 1471–1479.
16 Y. Sun, R. Liu, S. Wen, J. Wang, L. Chen, B. Yan, S. Peng, C. Ma, X. Cao, C. Ma, G. Duan, H. Wang, S. Shi, Y. Yuan and N. Wang, *ACS Appl. Mater. Interfaces*, 2021, **13**, 21272–21285.
17 L. A. Yousef, A. M. A. Morsy and M. S. Hagag, *Sep. Sci. Technol.*, 2020, **55**, 648–657.
18 R. Zhou, Z. Zhang, Z. Cheng, Y. Dai, Y. Liu, Y. Wang, Y. Xie, Z. Zhang, X. Cao and Y. Liu, *Environ. Nanotechnol., Monit. Manage.*, 2021, **15**, 100441.
19 C. Branger, W. Meouche and A. Margaillan, *React. Funct. Polym.*, 2013, **73**, 859–875.
20 L. Zhou, C. Shang, Z. Liu, G. Huang and A. A. Adesina, *J. Colloid Interface Sci.*, 2012, **366**, 165–172.
21 J. Qian, S. Zhang, Y. Zhou, P. Dong and D. Hua, *RSC Adv.*, 2015, **5**, 4153–4161.
22 H. Sarafraz, A. Minuchehr, G. H. Alahyarizadeh and Z. Rahimi, *Sci. Rep.*, 2017, **7**, 1–12.
23 S. Yang, J. Qian, L. Kuang and D. Hua, *ACS Appl. Mater. Interfaces*, 2017, **9**, 29337–29344.
24 Y. Yuan, Y. Yang, X. Ma, Q. Meng, L. Wang, S. Zhao and G. Zhu, *Adv. Mater.*, 2018, **30**, 1706507.
25 H. Ma, F. Zhang, Q. Li, G. Chen, S. Hu and H. Cheng, *RSC Adv.*, 2019, **9**, 18406–18414.
26 N. Li, P. Gao, H. Chen, F. Li and Z. Wang, *Chemosphere*, 2022, **287**, 132137.
27 S. Yang, G. Ji, S. Cai, M. Xu and D. Hua, *J. Radioanal. Nucl. Chem.*, 2019, **321**, 323–332.
28 N. He, H. Li, L. Li, C. Cheng, X. Lu, J. Wen and X. Wang, *J. Hazard. Mater.*, 2021, **416**, 126192.
29 J. F. Riordan, *Mol. Cell. Biochem.*, 1979, **26**, 71–92.
30 A. Echavarren, A. Galan, J. M. Lehn and J. De Mendoza, *J. Am. Chem. Soc.*, 1989, **111**, 4994–4995.
31 S. Nayab, H. Baig, A. Ghaffar, E. Tuncel, Z. Oluz, H. Duran and B. Yameen, *RSC Adv.*, 2018, **8**, 23963–23972.
32 T. Montanari, E. Finocchio, E. Salvatore, G. Garuti, A. Giordano, C. Pistarino and G. Busca, *Energy*, 2011, **36**, 314–319.
33 C. Zhou, A. Alshameri, C. Yan, X. Qiu, H. Wang and Y. Ma, *J. Porous Mater.*, 2013, **20**, 587–594.
34 L. Zhou, C. Shang, Z. Liu, G. Huang and A. A. Adesina, *J. Colloid Interface Sci.*, 2012, **366**, 165–172.
35 Y. Sun, Y. Wei, J. Pei, H. Nan, Y. Wang, X. Cao and Y. Liu, *Solid State Chem.*, 2021, **293**, 121792.
36 J. C. Edwards, C. Y. Thiel, B. Benac and J. F. Knifton, *Catal. Lett.*, 1998, **51**, 77–83.
37 C. S. Sridara, *Indian J. Chem. Technol.*, 2018, **25**, 353–360.
38 R. Kishor and A. K. Ghoshal, *Chem. Eng. J.*, 2015, **262**, 882–890.
39 B. Z. Zhan, M. A. White, M. Lumsden, J. Mueller-Neuhaus, K. N. Robertson, T. S. Cameron and M. Gharghouri, *Chem. Mater.*, 2002, **14**, 3636–3642.
40 Y. Zhang, T. Ye, Y. Wang, L. Zhou and Z. Liu, *J. Radioanal. Nucl. Chem.*, 2021, **327**, 1267–1275.
41 M. Su, Z. Liu, Y. Wu, H. Peng, T. Ou, S. Huang, G. Song, L. Kong, N. Chen and D. Chen, *Environ. Pollut.*, 2020, **268**, 115786.
42 M. K. Aroua, S. P. P. Leong, L. Y. Teo, C. Y. Yin and W. M. A. W. Daud, *Bioresour. Technol.*, 2008, **99**, 5786–5792.
43 Z. H. U. Mingyu, F. A. N. Dezhe, L. I. U. Bei, L. I. U. Shuya, F. A. N. G. Ming and T. A. N. Xiaoli, *J. Inorg. Mater.*, 2020, **35**, 309.
44 Q. Liang, J. Geng, H. Luo, W. Fang and Y. Yin, *J. Mol. Liq.*, 2017, **248**, 767–774.
45 M. A. Mahmoud, *Process Saf. Environ. Prot.*, 2016, **102**, 44–53.
46 Z. Sun, D. Chen, B. Chen, L. Kong and M. Su, *Colloids Surf., A*, 2018, **547**, 141–147.
47 Y. I. Jinxin, H. U. O. Zhipeng, T. A. N. Xiaoli, C. H. E. N. Changlun, A. M. Asiri, K. A. Alamry and L. I. Jiaxing, *Plasma Sci. Technol.*, 2019, **21**, 095502.
48 D. Ma, S. Hu, Y. Li and Z. Xu, *Sep. Sci. Technol.*, 2020, **55**, 1623–1635.
49 Y. A. Neolaka, Y. Lawa, J. N. Naat, A. A. P. Riwu, H. Darmokoesoemo, G. Supriyanto, C. I. Holdsworth, A. N. Amenaghawon and H. S. Kusuma, *React. Funct. Polym.*, 2020, **147**, 104451.